DOI 10.1007/s10812-018-0666-9
Journal of Applied Spectroscopy, Vol. 85, No. 3, July, 2018 (Russian Original Vol. 85, No. 3, May–June, 2018)

PULSE CATHODOLUMINESCENCE OF THE IMPURITY CENTERS IN CERAMICS BASED ON THE $MgAl_2O_4$ SPINEL

E. F. Polisadova, V. A. Vaganov,* S. A. Stepanov, V. D. Paygin, O. L. Khasanov, E. S. Dvilis, D. T. Valiev, and R. G. Kalinin

UDC 535.37:666.3.017

The spectral and luminescence decay kinetics of magnesium aluminate spinel ceramics prepared by spark plasma sintering (SPS) and the starting nanopowders were studied. It was demonstrated that two types of luminescence in spinel ceramics can be observed after pulse e-beam excitation. The first type is due to intrinsic defects, and the second type due to Cr^{3+} and Mn^{2+} ions. It was shown that the luminescence decay kinetics for Cr^{3+} and Mn^{2+} impurity ions can be approximated by the sum of two exponents. The decay times for the Cr^{3+} ion are 35 and 409 ns, for the Mn^{2+} ion are 29 and 340 ns. High-temperature exposure during SPS synthesis does not lead to a change in the nearest surroundings of impurity ions. In the luminescence spectra of ceramic and powder samples the intensity ratio changes of intrinsic and impurity centers is associated with strong diffuse scattering of light for spinel nanopowders.

Keywords: *pulse cathodoluminescence, nanoceramic, spinel $MgAl_2O_4$, Cr^{3+} ions, Mn^{2+} ions, spark plasma sintering technique, decay time.*

Introduction. Optically transparent magnesium aluminate spinel $MgAl_2O_4$ (MAS) ceramics due to a unique combination of physical and chemical properties (mechanical strength, thermal stability, resistance to corrosive media) is in demand in laser technology, aerospace engineering, security systems (transparent armor, etc.) [1], for passive optical components operating under extreme conditions [2]. Technologies for the synthesis of transparent ceramics are constantly being improved [3]. The properties of polycrystalline spinel depend on the pressing conditions (temperature, pressure, holding time, gaseous medium, etc.), morphology and particle size of the initial components of the charge, and their defect composition. The best optical performance results are achieved for the IR region, where the transmittance T is close to the characteristics of a single crystal and can be ~80%. At present, MAS is actively investigated as a material promising for applications as luminophores, scintillators, radiation converters [4–6]. Obviously, the presence of impurity centers in the structure of MAS has a significant effect on the optical-luminescence properties of the material. Several types of intrinsic defects have been known to exist in MAS: F and F^+-centers emitting in the "blue" region of the spectrum; F_2^+ -centers emitting in the UV region. Uncontrolled impurities in the composition of initial powders or impurities embedded in MAS ceramics during synthesis can affect the transfer of electronic excitations and create active absorption bands in various regions of the spectrum. For a purposeful change in luminescence properties, MAS crystals are activated by various kinds of impurities, including rare-earth ions [4, 5].

The purpose of this work is to study the spectral-kinetic characteristics of luminescence associated with impurity centers in nonactivated MAS ceramics synthesized under various conditions by the method of electropulse plasma sintering.

Experiment. Optically transparent ceramics are made from commercial MAS nanopowder (Baikalox, France). The granulometric composition of the nanopowder is determined by the laser diffraction method (Shimadzu, SALD-7101), according to which the average particle size is 37 nm. The specific surface area of 24.99 m^2/g was determined by the Brunauer–Emmett–Taylor method using a Sorbi-M instrument (Meta, Russia). Particle morphology was studied by scanning electron microscopy (SEM) (JEOL, JSM-7500FA). X-ray phase analysis of the initial nanopowder was performed using an XRD-7000S diffractometer (Shimadzu, Japan). The open source *PowderCell* software and international crystallographic database PDF-4 were employed to interpret the diffractograms.

*To whom correspondence should be addressed.

National Research Tomsk Polytechnic University, 30 Lenin Ave., Tomsk, 634050, Russia; email: vav13@tpu.ru. Translated from Zhurnal Prikladnoi Spektroskopii, Vol. 85, No. 3, pp. 407–412, May–June, 2018. Original article submitted December 12, 2017.

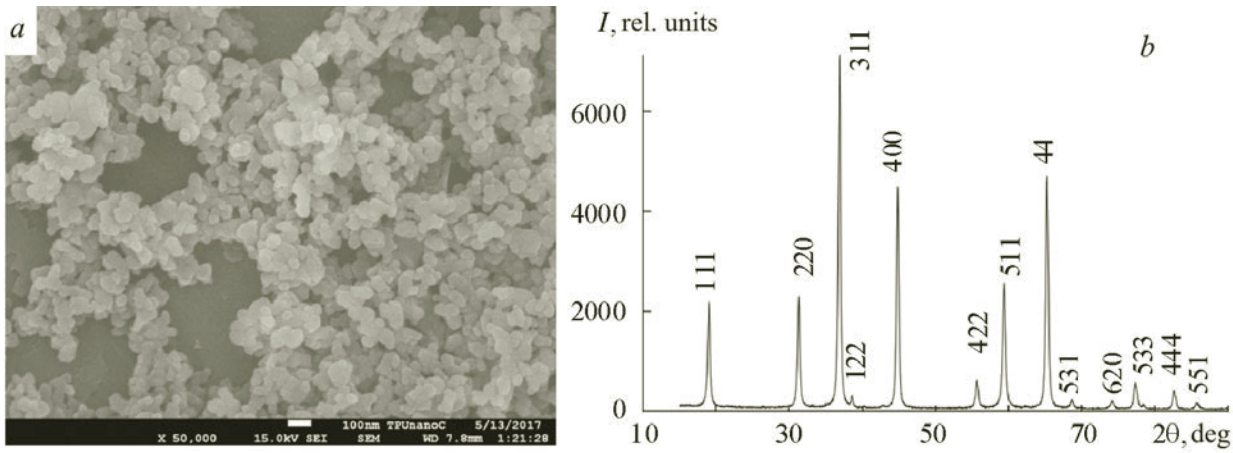

Fig. 1. SEM-image (a) and experimental diffraction pattern (b) of $MgAl_2O_4$ nanopowder.

Analysis of the SEM image (Fig. 1a) showed that the initial nanopowder consists of primary particles 20 to 273 nm in size, both primary particles and agglomerates measuring from tens to several hundreds of nanometers are observed. The content of oxygen-bound elements of the initial nanopowder corresponds to the stoichiometric composition of MAS (MgO 28.2%, Al_2O_3 71.8%). X-ray phase analysis confirmed that the investigated nanopowder consists of a stoichiometric MAS with a cubic crystal structure, and also exhibits an inappropriate ratio of the intensities of the main phase reflections, which may be due to the presence of residual alumina and magnesium oxide in the powder in the limits of <5.7 and <1.5 vol.%. Weak reflections in the regions of $2\theta = 42.9^o$ and 62.2^o confirm the presence of the MgO phase (lines of reflection from the (200) and (220) planes in magnesium oxide). Reflections corresponding to the aluminum oxide phase in the investigated range of diffraction angles coincide with the analytical lines of the MAS.

The size of coherent scattering regions (CSR) of the main phase was determined to be 37-nm by the Hall–Williamson X-ray diffraction broadening method, which is in good agreement with the results of laser diffraction and makes it possible to determine the degree of agglomeration of the powder up to 7.

Polycrystalline ceramics based on $MgAl_2O_4$ were obtained by the method of electropulse plasma sintering using the SPS-515S unit (Syntex Inc., Japan). The pressure of the powder pre-pressing in the graphite mold varied in the range of 60–83 MPa. Compacted samples were sintered in a vacuum (10^{-3} Pa) in the temperature range of 1300–1500°C with a constant heating rate of 50°C/min. The holding time at the maximum temperature for all samples was the same (10 min).

By sintering, transparent ceramic samples of a cylindrical shape with a height of 2.4–2.5 mm and a diameter of 20 mm were obtained. The density of the samples was determined by measuring their mass and linear dimensions. The ceramics were studied after their surfaces were mechanically polished with the EcoMet 300 Pro grinding and polishing system (Buehler, Germany) and MetaDi (Buehler, Germany) diamond slurries. The optical properties of samples in the UV, visible and near-IR regions were studied with SF-256 UVI (190–1100 nm) and SF-256 BIK (1000–2500 nm) double-beam scanning spectrophotometers. To excite cathodoluminescence (CL), a GIN-600 small-size high-current electron accelerator based on a vacuum diode was used, which is part of a pulsed optical spectrometer [7]. The accelerator is a source of electron pulses with a half-height duration of ~10 ns and an average energy of 250 keV. The excitation energy density can vary from 1 to 300 mJ/cm^2. Integral CL spectra were recorded with an AvaSpec-2048 optical fiber spectrometer (200–1100 nm), the time window of integration varied from 1 ms to 1 s. The CL spectrum was recorded after the action of a single electron pulse. Luminescence decay kinetics were determined with an FEU-106 photoelectric multiplier and a LECROY6030A digital oscilloscope.

Results and Discussion. The luminescence properties of the initial components for the synthesis of transparent ceramics (nanocrystalline powders) and $MgAl_2O_4$ ceramics samples themselves were investigated. Transmission in the near-IR region was ~30% and the thickness of the spinel sample was 1.5 mm (Fig. 2a). When the electron beam is used to excite spinel nanocrystals and ceramic samples, luminescence is observed in the visible spectral range. In CL spectra of polycrystalline spinel $MgAl_2O_4$ and nanocrystalline spinel powder (Fig. 2b), a broad band is observed in the "blue" region (λ_{max} = 420 nm) along with a series of narrow lines in the red region. A weak maximum at 525 nm can also be identified.

For ceramics samples there is a change in the ratio of the luminescence intensity in the "blue" and "red" regions. Broadband luminescence in the luminescence spectrum with λ_{max} = 420 nm can be due to the emission of several types

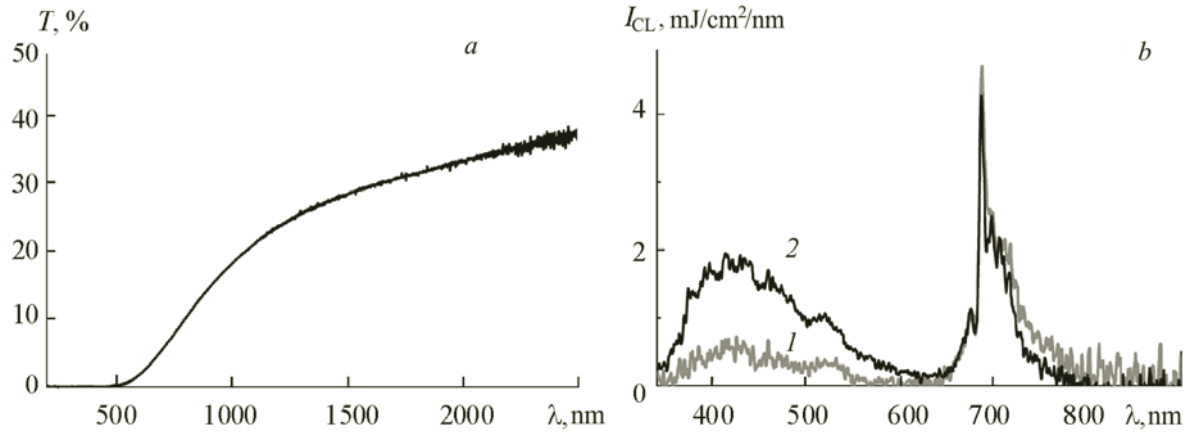

Fig. 2. Direct transmittance spectrum of a sample of $MgAl_2O_4$ spinel synthesized by electropulse plasma sintering (a); cathodoluminescence spectrum of $MgAl_2O_4$ spinel in the form of powder (1) and ceramics (2) (b).

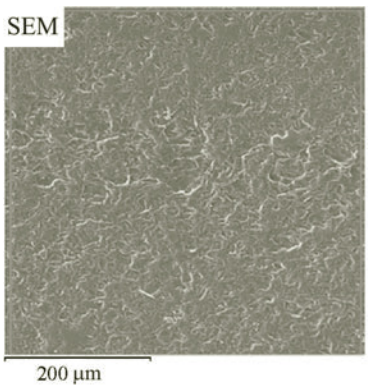

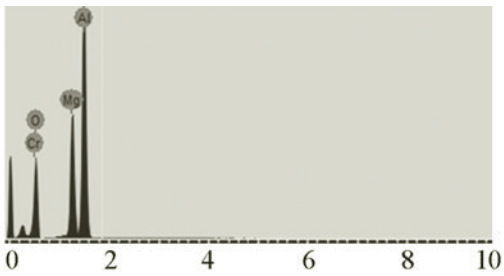

Element	wt. %	at. %
O	38.48	50.54
Mg	18.46	15.95
Al	42.98	33.48
Cr	0.08	0.03
Total	100.00	–

Fig. 3. Energy dispersive analysis of a sample of polycrystalline spinel $MgAl_2O_4$ synthesized by the method of electropulse plasma sintering.

of "intrinsic" luminescent centers, oxygen vacancies with one or two trapped electrons, F^+- and F-centers [8]. In addition, antidefects (Mg_{Al}, Al_{Mg}), complex defects in the form of associations of oxygen vacancies with intrinsic or impurity defects, were found in spinel crystals [9].

It is known that in the composition of non-activated MAS there are impurities of the iron group and elements such as V, Cr, Mn, Co, Ti, Fe [9, 10], as well as Cu and other impurities. Impurity defects can act as luminescence centers. Cr^{3+} ions emit near 1.8 eV [4, 10], the emission of V^{3+} and Mn^{2+} ions in the tetrahedral position can be recorded near 2.38 eV [10] similarly to MgO oxide containing Cu. The centers associated with copper ions emit near 3.0 eV. The presence of Fe^{3+} ions in the octahedral position is identified by the presence of absorption bands near 4.8 and 6.4 eV [10].

Identification of impurity luminescence centers in MAS is often difficult due to strong overlap with the luminescence of intrinsic defects. When excited by a pulsed electron beam of nanosecond duration, a series of narrow lines in the "red" region of the spectrum (686, 698, 708, 716 nm) associated with chromium ions is effectively excited [4, 10]. Chromium ions in spinel crystals take the charged state of Cr^{3+} ions (electron configuration d^3) and isomorphically replace aluminum ions in trigonally distorted octahedra [11]. According to the data in [12], the luminescence in the 1.6–2.2 eV region can also be associated with impurity Ti^{3+} ions, but most studies confirm that a series of lines in the red region are due to trivalent chromium ions. This luminescence is characteristic both for nanocrystals and for ceramic spinel samples. The results of

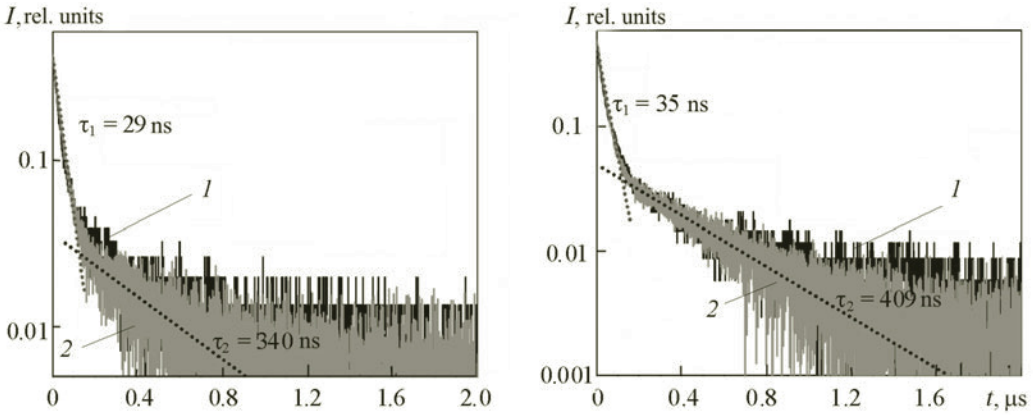

Fig. 4. Cathodoluminescence decay kinetics of impurity ions of manganese (a) and chromium (b) in magnesium aluminate spinel ceramics (1) and nanopowder (2); λ_{rad} = 520 (a) and 686 nm (b).

energy-dispersive analysis (EDA) of ceramics show the presence of chromium in an amount of 0 to 0.03 at.% in various zones of the sample. Figure 3 shows the data of EDA in one of the zones of a transparent ceramics sample.

Impurity Cr^{3+} ions have been detected in nominally pure spinel crystals [13, 14] at a concentration of ~1–10 ppm. The effect of MAS composition on the spectral characteristics of chromium ions is known: an increase in the fraction of Al_2O_3 leads to a monotonic shift of the chromium absorption bands towards longer wavelengths. A similar effect is observed with increasing chromium content: in the $MgAl_2O_4 \leftrightarrow MgCr_2O_4$ series, the crystal lattice parameter increases and the absorption bands shift toward longer wavelengths. In this case, the spectral position of the main chromium line — the *R*-line (^2E_g–$^4A_{2g}$ transition) — depends to some extent on the strength of the crystal field and the nearest environment. For a nominally pure single crystal, according to [13, 14], the maximum wavelength of the luminescence of chromium ions is 693 nm. The presence of defects of various types in the nearest environment of chromium ions affects their spectroscopic characteristics. This property is used to estimate the inversion parameter of stoichiometric spinel crystals by determining the cationic environment of chromium ions. According to [15], in the spectra of natural spinel crystals at the temperature of liquid nitrogen, the doublet structure of the chromium *R*-line can be observed. For an artificial spinel, the chromium lines are considerably broadened and no splitting is observed either at room temperature or at nitrogen temperature.

The results of our studies show that the spectral characteristics of chromium ions in nanocrystalline spinel with particle sizes of 20–273 nm and in transparent ceramics obtained by electroplasma sintering are identical. At ceramics synthesis temperatures of 1400°C in air, the cationic environment of chromium ions does not change. The experimental data obtained in our investigations were in good agreement with the results of calculations and spectroscopic measurements in [6], in which $MgAl_2O_4$:Cr^{3+} nanopowders were investigated. According to [6], chromium ions occupy the position of Al^{3+} in the lattice with point symmetry D_{3d}, the energy levels of Cr^{3+} are split by a trigonal crystal field. The observed change in the relationship between the luminescence of "intrinsic" centers and the luminescence of chromium ions is apparently due to the presence of diffuse scattering in the blue region of the spectrum for spinel samples in the form of nanopowders.

The kinetics of the decay of chromium luminescence in MAS nanoparticles in free and consolidated (in the form of ceramics) states have also been studied. The results show that the luminescence decay patterns of Cr^{3+} ions in $MgAl_2O_4$ nanocrystals and ceramic samples (Fig. 4b) are identical. The decay kinetics in the microsecond range is satisfactorily described by the sum of two exponentials with characteristic times $\tau_1 \approx 35$ ns and $\tau_2 \approx 409$ ns.

The emission maximum in the range of 520–525 nm, recorded in the CL spectra of MAS, can be associated with the presence of Mn^{2+} impurity ions [10]. Manganese ions can be in both tetra- and octahedral positions. In artificial MAS crystals, the concentration of Mn^{2+} ions can be ~10–55 ppm. It is known that in artificial samples doped with manganese or in natural spinel crystals in optical spectra, bands corresponding to transitions in the Mn^{2+} ion in the tetrahedral position are observed [15]. The introduction of anionic vacancies causes a redistribution of Mn^{2+} radiation, which includes the "green" emission associated with tetrahedral Mn^{2+}, and the "red" emission related to octahedral Mn^{2+} [16]. The stoichiometric spinel, activated by Mn^{2+}, emits only red light with a wavelength of 650 nm. In natural spinel crystals, the emission band of Mn^{2+} is observed only at 620 nm, whereas in synthetic crystals it is observed at 516 nm [15]. In [17], the asymmetric shape of the

green band of Mn^{2+} is described by two closely overlapping bands at 2.43 eV (511 nm) and 2.39 eV (518 nm). These bands are related to changes in the second coordination sphere of the nearest neighbors of the manganese ion in the tetrahedral position. In the investigated spinel samples, the emission of the manganese ion is observed in the tetrahedral position (Fig. 2b). Luminescence decay at 525 nm occurs in the microsecond range (Fig. 4a), with electronic excitation the kinetics is described by the sum of two exponential components with the times 29 and 340 ns.

The authors of [18] found that oxygen vacancies affect radiation intensity at 525 nm. When annealing in argon atmosphere, an increase in the intensity of this band is observed, while annealing in oxygen leads to a decrease in this intensity. It is possible that the presence of oxygen vacancies has an effect on the emission intensity of manganese. The process of excitation energy transfer to manganese ions through oxygen is justified in [19]. Correlation of the emission intensity of manganese ions with the concentration of oxygen vacancies may indicate the formation of associations of manganese centers with oxygen vacancies [20].

Conclusions. The spectral-kinetic characteristics of cathodoluminescence of magnesium aluminate spinel nanocrystals and ceramics synthesized by the method of electropulse plasma sintering were investigated. It was found that when the electron beam acts on the samples of nonactivated spinel $MgAl_2O_4$, the impurity ions Cr^{3+} and Mn^{2+} are excited. It was shown that luminescence decay kinetics of impurity ions of chromium and manganese in the spinel structure does not depend on the structural state. High-temperature exposure in the process of electropulse sintering does not lead to a change in the nearest environment of impurity ions Cr^{3+} and Mn^{2+}. Two-stage kinetics of luminescence is observed, decay occurs within a few microseconds. It was shown that for spinel samples in the form of nanopowders and ceramics the ratio of the emission intensity of impurity and intrinsic centers varies.

Since spinels are used as luminophores, scintillators, laser materials, it is necessary to take into account in nominally pure samples of magnesium aluminate spinel the presence of Cr^{3+} and Mn^{2+} impurity defects that exert a significant influence on its optical-luminescent properties and excitation energy transfer processes.

Acknowledgment. The work was supported by the Russian Science Foundation (Project No. 17-13-01233).

REFERENCES

1. E. S. Lukin, N. A. Popova, V. S. Glazachev, L. T. Pavlyukova, and N. A. Kulikov, *Zh. Konstr. Kompoz. Mater.*, No. 3, 24–36 (2015).
2. J. Zhang, T. Lu, X. Chang, N. Wei, and W. Xu, *J. Phys. D: Appl. Phys.*, **42**, No. 5, 520–535 (2009).
3. O. L. Khasanov, E. S. Dvilis, and Z. G. Bikbaeva, *Methods of Compacting and Consolidating Nanostructured Materials and Products* [in Russian], Moscow, Binom (2013).
4. S. V. Motloung, B. F. Dejene, R. E. Kroon, O. M. Ntwaeaborwa, H. C. Swart, and T. E. Motaung, *Optik*, **131**, 705–712 (2017).
5. C.-F. Chen, F. P. Doty, R. J. T. Houk, R. O. Loutfy, H. M. Volz, and P. Yang, *J. Am. Ceramic Soc.*, **93**, No. 8, 2399–2402 (2010).
6. M. G. Brik, J. Papan, D. J. Jovanović, and M. D. Dramićanin, *J. Lumin.*, **177**, 145–151 (2016).
7. V. F. Tarasenko, V. M. Lisitsyn, E. F. Polisadova, D. T. Valiev, A. G. Burachenko, and E. H. Baksht, *Luminescence of the Calcite under E-Beam Excitation* (2012), pp. 193–211.
8. G. S. White, K. H. Lee, and J. R. Crawford, *J. Appl. Phys. Lett.*, **35**, 1–3 (1979).
9. P. D. Borges, J. Cott, F. G. Pinto, J. Tronto, and L. Scolfaro, *Mater. Res. Express*, **3**, 762–772 (2016).
10. P. K. Bandyopadhyay and G. P. Summers, *J. Phys. Rev.*, **31**, 422–431 (1985).
11. D. L. Wood, G. F. Imbusch, R. M. Macfarlane, P. Kisliuk, and D. M. Larkin, *J. Chem. Phys.*, **48**, No. 11, 5255–5263 (1968).
12. D. Lapraz, P. Iacconi, D. Daviller, and B. Guilhot, *J. Phys. Status Solidi*, **126**, 521–531 (1991).
13. C. Ballesteros, J. Llopis, and R. Y. González, *J. Solid State Commun.*, **51**, No. 1, 37–39 (1984).
14. Yu. G. Kazarinov, V. T. Gritsyna, and V. A. Kobyakov, *Voprosy atomnoj nauki i tekhniki. Ser. Fizika Rad. Povrezhdenij i Rad. Materialovedenie* (*Problems of Nuclear Science and Technology*. *Ser. Radiation Damage Physics and Radiation Technology*), **81**, No. 3, 53–57 (2002).
15. D. T. Sviridov, R. K. Sviridova, and Yu. F. Smirnov, *Optical Spectra of Ions of Transition Metals in Crystals* [in Russian], Nauka, Moscow (1976).
16. A. Tomita, T. Sato, K. Tanaka, Y. Kawabe, M. Shirai, K. Tanaka, and E. Hanamura, *J. Lumin.*, **109**, No. 1, 19–24 (2004).

17. K. Izumi, S. Miyazaki, S. Yoshida, T. Mizokawa, and E. Hanamura, *Phys. Rev. B*, **76**, No. 7, 075111 (2007).
18. U. R. Rodriguez-Mendoza, V. D. Rodriguez, and A. Ibarra, *Radiat. Effect. Defect. Solids*, **136**, No. 2, 29–32 (1995).
19. M. L. Gaft, B. S. Gorobets, and I. S. Naumova, *Mineralog. Zh.*, **3**, No. 2, 71–80 (1981).
20. C. A. Gilbert, R. Smith, S. D. Kenny, S. T. Murphy, and R. W. Grimes, *J. Phys.: Condens. Matter*, **21**, No. 27, 275406 (2009).